

Interactive comment on “Hazard Assessment Comparison of Tazhiping Landslide Before and After Treatment” by Dong Huang et al.

Dong Huang et al.

dhuang@imde.ac.cn

Received and published: 26 July 2017

Response to Reviewer Comments

Manuscript title: (the title: Hazard Assessment Comparison of Tazhiping Landslide Before and After Treatment Using the Finite Volume Method) Manuscript number: 2016-391 Thanks very much for reviewer’s comments, which helped us to improve the quality of manuscript. We have made major revisions to address the comments raised by the reviewer. The following responses have been prepared to address reviewer’s comments in a point-by-point fashion. All changes have been marked with BULE in the revised manuscript. We would be happy to make further modifications if required. We hope the changes listed have made the manuscript suitable for publication, and we

[Printer-friendly version](#)

[Discussion paper](#)



look forward to your response.

General comments

Q1: You followed the indications given by both reviewers and you corrected and improved your manuscript accordingly. Most of the questions are answered and changes and completions are made. But the paper is still of fair quality only. Some information is given in the wrong chapters. You talk about "confusion" in the chapter "Conclusions and discussion" but your revision does not really solve the problem. Please introduce these points in the "Introduction"! .

A1: We acknowledge the remark of the reviewer. We tried our best to improve the manuscript. We earnestly appreciate the editors/reviewers' work and hope that the corrections meet their approval. We totally agree with the reviewer. We have move p. 20 lines 373 - 380 to the section "Empirical prediction method". This would help to avoid the confusion about the mass movement process that is discussed in the Methods section. Please see p.2 line 64-70.

Q2: The content of the manuscript is now more or less OK. All necessary information is given. Figures could still be improved. The comparison between pre and post treatment results could be solved easily introducing some additional lines of main results from the pre simulations in the figures of the post simulations (e.g. with a dotted dark line or similar).

A2: We appreciate the comments. We have carefully revise the whole manuscript to follow strictly the reviewers comments as much as possible. Figure.7a has been extensively revised. Please see p.13, line 289. We have re-organized and added more information about the comparison between pre and post treatment results. Please see p.16, line 330 (Figure.9a) and see p.22, line 388 (Figure.10b).

Q3: Abstract: 3 times "adopted", poor linguistic quality, please reformulate and improve.

A3: Thank you for the insightful comments. We have re-organized and improved the abstract of the manuscript. Please see the abstract section in the new version of the manuscript.

Q4: Introduction: still not enough information to avoid the confusion that the authors mention in the Conclusions and discussions. Please introduce these points mentioned in the chapter "Conclusions and discussion" here. p.2, line 58: why not move this information to the section "Empirical prediction method"?

A4: Thank you for pointing out the problem. I have move this information to the section "Empirical prediction method". Please see p.2 line 64-70 and A.1.

Q5: Methods: I somewhat miss information about the method used to do the hazard prediction and the evaluation of the dynamic interaction with buildings. Shouldn't that be introduced here?

A5: We have introduced the method used to do the hazard prediction and the evaluation of the dynamic interaction with buildings. Please see p.7 line 198-204 in the new version of the manuscript.

Q6: Study area and data: Fig. 4: What defines the blue outline of the landslide area. Is this perimeter based on field survey?

A6: Yes, it is based on the survey report and field investigation. Please see Figure.4.

Q7: Results:I miss a proper comparison between model result and reality, e.g. outline of the landslide indicated in fig. 7 . A comparison between the two situations would be interesting. p13, line 283: delete "speed" and check blanks between words in the line above

A7: We have added more information about the comparison between model result and reality. Please see Figure.9a and Figure.10b. Thank you for the correction. It has been deleted and deleted the blanks between words in the line above. Please see p.15, line 301 and 302.

[Printer-friendly version](#)

[Discussion paper](#)



Q8: Conclusions and discussion: I propose to move lines 373 - 380 to the Introduction (and repeat it partially in the conclusions). This would help to avoid the confusion about the mass movement process that is discussed in the Methods section. Also, the section about the selection of model parameters has to be introduced much earlier. This is the motivation for this paper and has to be mentioned in the Introduction.

A8: Thank you for the insightful comments. We have move p. 20 lines 373 - 380 to the section "Empirical prediction method" and simply to introduce about the selection of model parameters in the Introduction. Please see p.2 line 64-71.

The text of the manuscript has been revised.

Interactive comment on Nat. Hazards Earth Syst. Sci. Discuss., <https://doi.org/10.5194/nhess-2016-391>, 2017.

Printer-friendly version

Discussion paper



Hazard Assessment Comparison of Tazhiping Landslide Before and After Treatment using the Finite Volume Method

Dong Huang¹, YuanJun Jiang^{1*}, JianPing Qiao¹, Meng Wang¹

1. Key Laboratory of Mountain hazards and Surface process, Institute of Mountain hazards and Environment, Chinese Academy of Science, Chengdu 610041, China

*Corresponding author (yuanjun.jiang.civil@gmail.com).

Abstract: Through investigation and analysis of geological conditions and mechanical parameters of the Tazhiping landslide, the finite volume method was adopted, and coupling with Vollmy model the rheological model was adopted used to simulate the landslide and avalanche entire mass movement process. The present paper adopted adopts the numerical approach of RAMMS and the GIS platform to simulate the mass movement process before and after engineering treatment. This paper also provides the conditions and characteristic variables parameters of flow-type landslide mass flow in terms of soil deposits (flow height, velocity, and stresses) during the landslide mass movement process and mapped the 3D division of hazard zones before and after engineering landslide treatment was also mapped. The results indicated that the scope of hazard zones decreased contracted after engineering treatment of the landslide. Compared with the case of before engineering treatment, the extent of high-hazard zones was reduced by about 2/3 of the area before treatment, and the characteristic variables parameters of the mass movement process in the case of after treatment decreased to 1/3 of those in the case of before treatment. Despite having engineering treatment, the Tazhiping landslide still poses significant potential threat hazard to the nearby settlements residences. Therefore, it suggests we propose that the houses located in high-hazard zones should be relocated or reinforced for protection.

Keywords: finite volume method; rheological model; motion feature parameters; hazard assessment

1. Introduction

The hazards of a landslide include scope of influence (i.e., source area, possible path area, and backward and lateral expansion area) and secondary disasters (i.e., reservoir surge, blast, and landslide-induced barrier lake). A typical landslide hazard assessment aims to propose a systematic hazard assessment method with regard to a given position or a potential landslide. Current research on typical landslide hazard assessment remains immature, and there are multiple methods for interpreting landslide hazards. To be specific, the scope of influence prediction of a landslide refers to deformation and instability characteristics such as sliding distance, movement speed, and bulking thickness range. The movement behavior of a landslide

[a1]: Answer to the comment Q3: We have re-organized and improved the abstract of the manuscript.

44 mass is related to its occurrence, sliding mechanisms, mass characteristics, sliding
45 path, and many other factors. Current landslide movement prediction methods include
46 empirical prediction and numerical simulation.

47 **Empirical prediction method:** The empirical prediction method involves
48 analyzing landslide flow through the collection of landslide parameters in the field. It
49 further consists of the geomorphologic method (Costa, 1984; Jackson et al., 1987;
50 Scott et al., 1993), the geometric change method (Finlay et al., 1999; Michael-Leiba et
51 al., 2003), and the volume change method (Fannin et al., 2001). Empirical models are
52 commonly simple and easy to apply, and the required data are easy to obtain as well.

53 **Numerical simulation method:** Numerical simulation methods are further divided
54 into the continuous deformation analysis method (Hung, 1995; Evans et al., 2009;
55 Wang, et al., 2016), the discontinuous deformation analysis method (Shi, 1988), and
56 the simplified analytical simulation method (Christen et al., 2010a; Sassa, 2010;
57 Bartelt et al., 2012; Du et al., 2015). The numerical simulation method expresses
58 continuous physical variables using the original spatial and temporal coordinates with
59 geometric values of discrete points. Numerical simulations follow certain rules to
60 establish an algebraic equation set in order to obtain approximate solutions for
61 physical variables.

62 Empirical prediction models only provide a simple prediction of the sliding path.
63 Due to the differences in geological environments, empirical prediction models
64 commonly have low generality. Landslides move downslope in many different ways
65 (Varnes, 1978). In addition, landslides can evolve into rapidly travelling flows, which
66 exhibit characteristics of debris flows on unchannelized or only weakly channelized
67 hillslopes. The geomorphic heterogeneity of rapid shallow landslides, such as
68 hillslope debris flows, is larger than observed in channelized debris flows; however
69 many of these flows can be successfully modelled using the Voellmy-fluid friction
70 (Christen et al., 2012). The selection of model parameters remains one of the
71 fundamental challenges for numerical calculations of natural hazards.

72 The continuous deformation method has the advantage of an extremely strong
73 replication capability, but it is not recommended when analyzing flow-type landslides,
74 lahars, or debris flows because of complicated rheological behaviors (Iverson et al.,
75 1997, 2001; Hung et al., 2001; Glade 2005; Portilla et al., 2010; Chen et al., 2014).
76 The fluid mechanics-based discontinuous deformation method has several
77 shortcomings such as, great computational burden, difficult parameter selection, and
78 difficult 3D implementation. The simplified analytical simulation method fully takes
79 into account the flow state properties of landslides before introducing a rheological
80 model and can easily realize 3D implementation on the GIS platform. On that account,
81 this paper adopted the continuous fluid mechanics-based finite volume method
82 (simplified analytical simulation method). We introduce a rheological model on the
83 basis of using mass as well as momentum and energy conservation to describe the
84 movement of landslides. We also employed GIS analysis to simulate the entire
85 movement process of Taziping landslide and map the 2D division of hazard zones.

86

87 2. Methods

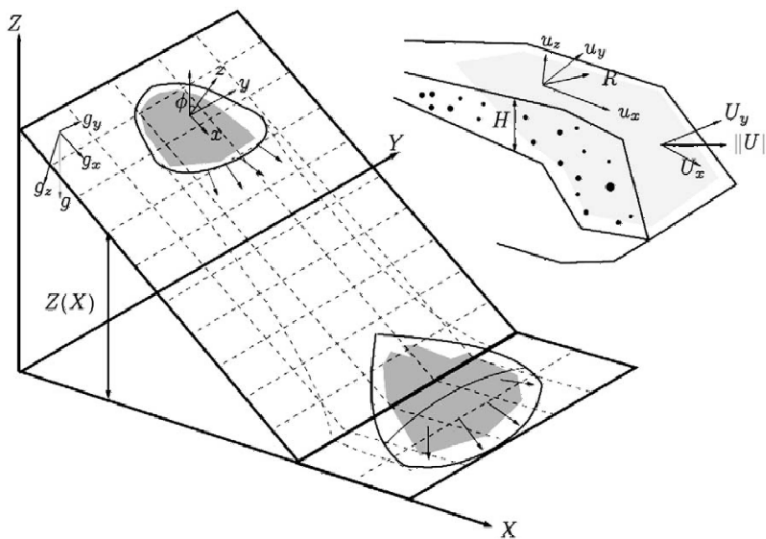
[a2]: Answer to the comment Q1 and Q4: We have move p. 20 lines 373 - 380 to the section "Empirical prediction method". This would help to avoid the confusion about the mass movement process that is discussed in the Methods section.

[a3]: Answer to the comment Q8: We have simply to introduce about the selection of model parameters in the Introduction section.

88 **2.1 Kinetic analysis method**

89 Adopting the continuous fluid mechanics-based finite volume method, this paper
90 took into account erosion action on the lower surface of the sliding mass and the
91 change in frictional resistance within the landslide-debris flow in order to establish a
92 computational model. The basic idea is to divide the calculation area into a series of
93 non-repetitive control volumes, ensuring that there is a control volume around each
94 grid point. Each control volume is then integrated by the unresolved differential
95 equation in order to obtain a set of discrete equations. The unknown variable is the
96 numerical value of the dependent variable at each grid point. To solve the integral of a
97 control volume, we make a hypothesis about the change rule of values among grid
98 points, that is, about their piecewise distribution profile. The finite volume method
99 can satisfactorily overcome the finite element method's weakness of slow calculation,
100 and solve the problem of complex region processing. Thus, we adopted the finite
101 volume method to establish the kinematic model for the landslide flow process.

102 The core of the finite volume method is domain discretization. The finite volume
103 method uses discrete points as a substitute for continuous space. The physical
104 meaning of the discrete equation is the conservation of the dependent variable in a
105 finite control volume. Establishment of the conservation equation is based on the
106 continuous movement model, that is, the continuity hypothesis about landslide
107 substances. We divided the landslide mass into a series of units and made the
108 hypothesis that each unit has consistent kinematic parameters (speed at a depth,
109 density, etc.) and physical parameters (Fig.1). We also established an Eulerian
110 coordinate system-based conservation equation with regard to each control volume.



111

112 Fig.1 Schematic diagram of finite volume discretization (Christen et al., 2010a).

113 **2.2 Control equation**

114 The computational domain is defined as directions x and y , and the

115 topographic elevation is given the coordinate $z(x, y)$. $H(x, y, t)$ is assumed as the
 116 change relationship of landslide thickness with time; $U_x(x, y, t)$ and $U_y(x, y, t)$
 117 respectively represent the mean movement speeds along directions x and y at
 118 moment t ; $n_x = U_x / \sqrt{U_x^2 + U_y^2}$ and $n_y = U_y / \sqrt{U_x^2 + U_y^2}$ represent the cosinoidal and
 119 sinusoidal flow vectors of the landslide on the plane $x - y$. The mean flow speed of
 120 substances is defined as $U = \sqrt{U_x^2 + U_y^2}$.

121 Thus, the mass balance equation becomes:

$$122 \quad \partial_t H + \partial_x (HU_x) + \partial_y (HU_y) = \dot{Q} \quad (1)$$

123 wherein, $\dot{Q}(x, y, t)$ represents the change rate (entrainment rate) of landslide
 124 volume with time.

125 Assuming that $l(x, y, t)$ represents the movement distance of the landslide with
 126 time, we can obtain:

$$127 \quad \dot{Q} = \begin{cases} 0 & \text{if } h_i = 0 \\ \frac{\rho_i}{\rho_a} h_i \frac{U}{l} & \text{if } k_i l \geq h_i \\ \frac{\rho_i}{\rho_a} k_i U & \text{if } k_i l < h_i \end{cases} \quad (2)$$

128 wherein, h_i represents the thickness of the i th layer of the landslide in the
 129 movement process; ρ_i represents the density of the i th layer of the landslide in the
 130 movement process; ρ_a represents the density of the landslide; the dimensionless
 131 parameter k_i represents the entrainment rate.

132 The momentum balance equation is:

$$133 \quad \partial_t (HU_x) + \partial_x (HU_x^2 + \frac{g_x k_{a/p} H^2}{2}) + \partial_y (HU_x U_y) = S_{gx} - S_f(R)[n_x] \quad (3)$$

$$134 \quad \partial_t (HU_y) + \partial_y (HU_y^2 + \frac{g_y k_{a/p} H^2}{2}) + \partial_x (HU_x U_y) = S_{gy} - S_f(R)[n_y] \quad (4)$$

135 wherein, $S_{gx} = g_x H$ and $S_{gy} = g_y H$ represent the dynamic components of the

136 acceleration of gravity in directions x and y ; $g=(g_x \ g_y \ g_z)$ represents the
 137 vector of the acceleration of gravity; k_{ap} represents the pressure coefficient of soil;
 138 ρ_a represents the density of the landslide; the dimensionless parameter k_i
 139 represents the entrainment rate; $S_f(R)$ represents the frictional resistance.

140 The kinetic energy balance equation is:

$$141 \quad \partial_t(HR) + \partial_x(HRU_x) + \partial_y(HRU_y) = \dot{P} - \dot{D} \quad (5)$$

142 wherein, $R(x, y, t)$ represents the random mean kinetic energy of the landslide;
 143 $\dot{P}(x, y, t)$ and $\dot{D}(x, y, t)$ represent the random increased kinetic energy and decreased
 144 kinetic energy of the landslide.

145 2.3 Constitutive relationship

146 The improved Voellmy rheological model is applied in the computational
 147 simulation of the landslide. See the computational formula below:

$$148 \quad S_f = \frac{u_i}{\|U\|} (h\mu g_z + R_i U^2 + R_\zeta U^2) \quad (6)$$

$$149 \quad R_i = \mu h \frac{U^T K U}{U^2}, R_\zeta = \frac{g}{\zeta} \quad (7)$$

150 wherein, $u_i/\|U\|$ represents the unit vector in the movement direction of the
 151 landslide; μ represents the Coulomb friction coefficient, and is related to $R(x, y, t)$,
 152 the random mean kinetic energy of the landslide; R_i represents the gravity-related
 153 frictional force coefficient; K represents the substrate surface curvature; ζ
 154 represents the viscous friction coefficient of the “turbulent flow”.

155 2.4 HLL-Heun numerical solution

156 Synthesizing control equations (1), (3), (4) and (5), we can obtain the simplified
 157 form of the nonlinear hyperbola equation:

$$158 \quad \partial_t V + \nabla \cdot F(V) = G(V) \quad (8)$$

$$159 \quad V = \begin{pmatrix} H \\ HU_x \\ HU_y \\ HR \end{pmatrix} \quad G(V) := \begin{pmatrix} \dot{Q} \\ S_{gx} - S_{fx} \\ S_{gy} - S_{fy} \\ \dot{P} - \dot{D} \end{pmatrix}$$

160

$$F(V) = \begin{pmatrix} HU_x & HU_y \\ HU_x^2 + g_z k_{ap} \frac{H^2}{2} & HU_x U_y \\ HU_x U_y & HU_y^2 + g_z k_{ap} \frac{H^2}{2} \\ HRU_x & HRU_y \end{pmatrix}$$

161

wherein, $V(x, y, t)$ represents a vector equation consisting of four unknown

162

vector variables; $F(V)$ represents the flux function; $G(V)$ represents the source

163

term. Based on the HLLE equation of the finite volume method and the quadrilateral

164

grid, the node layout can adopt the grid center pattern, and the normal flux along one

165

side of the control volume can be represented by the flux at the center of the side. The

166

finite volume discretization adopting the control volume as unit is depicted in Fig.1;

167

the Gauss theorem can be followed for the integration of equation (8), wherein C_i

168

represents the unit volume; after converting the volume integral flux function $F(V)$

169

into the curved surface integral, we can obtain:

170

$$\int_{C_i} \partial_t V dx + \iint_{\partial C_i} F(V) \cdot n_i d\sigma = \int_{C_i} G(V) dx \quad (9)$$

171

wherein, n_i represents the outward normal direction vertical to unit C_i at the

172

boundary; through adopting the HLL format for the discretization of surface integral,

173

the following simplified form can be obtained:

174

$$V_i^{(*)} = V_i^{(n)} + \frac{\Delta t}{A_{C_i}} \Delta F_i^{(HLL)}(V^{(n)}) \quad (10)$$

175

$$V_i^{(**)} = V_i^{(*)} + \frac{\Delta t}{A_{C_i}} \Delta F_i^{(HLL)}(V^{(*)}) \quad (11)$$

176

$$V_i^{(n+1)} = \frac{1}{2} (V_i^{(n)} + V_i^{(**)}) \quad (12)$$

177

wherein, $V_i^{(n)}$ represents the mean value of unit variables at moment $t^{(n)}$; $V^{(n)}$

178

represents the mean value of the entire grid at moment $t^{(n)}$; $\Delta t := t^{(n-1)} - t^{(n)}$ represents

179

the calculated time step; A_{C_i} represents the area of unit C_i ; $\Delta F_i^{(HLL)}$ represents the

180

approximate value of the curved surface integral, as shown below:

181

$$\Delta F_i^{(HLL)}(V^{(n)}) := - \sum_{j=1}^4 F_{ij}^{(HLL)}(V^{(n)}) n_{ij} \Delta X \quad (13)$$

182

wherein, n_{ij} represents the outward normal direction of the i th unit at

183 boundary j ; the flux calculation term $F_{ij}^{(HLL)}(V^{(n)})$ represents the approximate
 184 solution mode of the Riemann problem of the i th unit at boundary j ; see the
 185 computational formula below:

$$186 \quad F_{ij}^{(HLL)}(V^{(n)}) = \begin{cases} F(V_L^{(n)}) & 0 \leq S_L \\ \frac{S_R F(V_L^{(n)}) - S_L F(V_R^{(n)}) + S_R S_L F(V_R^{(n)} - V_L^{(n)})}{S_R - S_L} & S_L \leq 0 \leq S_R \\ F(V_R^{(n)}) & S_R \leq 0 \end{cases} \quad (14)$$

187 wherein, $V_L^{(n)}$ and $V_R^{(n)}$ respectively represent the approximate values of $V^{(n)}$
 188 on both sides of boundary j of the i th unit; S_L and S_R respectively represent the
 189 wave speeds on the left and right sides. Refer to the computational method described
 190 by Toro (1992). In addition, the gradient magnitude in the original second-order
 191 difference equation can be limited through multiplication with the flux limiter, and the
 192 second-order format of the TVD property can be constructed to avoid the occurrence
 193 of numerical oscillation. Refer to the specific method described by LeVeque (2002).

194 In this paper a numerical solver within RAMMS is used, which was specifically
 195 designed to provide landslide (avalanche) engineers with a tool that can analyze
 196 problems with two-dimensional depth-averaged mass and momentum equations on
 197 three-dimensional terrain using both first and second-order finite volume methods
 198 (Christen et al., 2010b). Therefore, the finite volume method is adopted to analyze the
 199 the flow-type (high mobility, high velocity, large scope of risks, etc.) of the landslide
 200 mass movement process. The present paper adopts the numerical approach of
 201 RAMMS and the GIS platform to simulate the mass movement process before and
 202 after treatment. The landslide depositional characteristics and the mass movement
 203 conditions can be combined to provide a scientific basis for engineering prevention,
 204 control, and forecast risk assessments for these kinds of disasters.

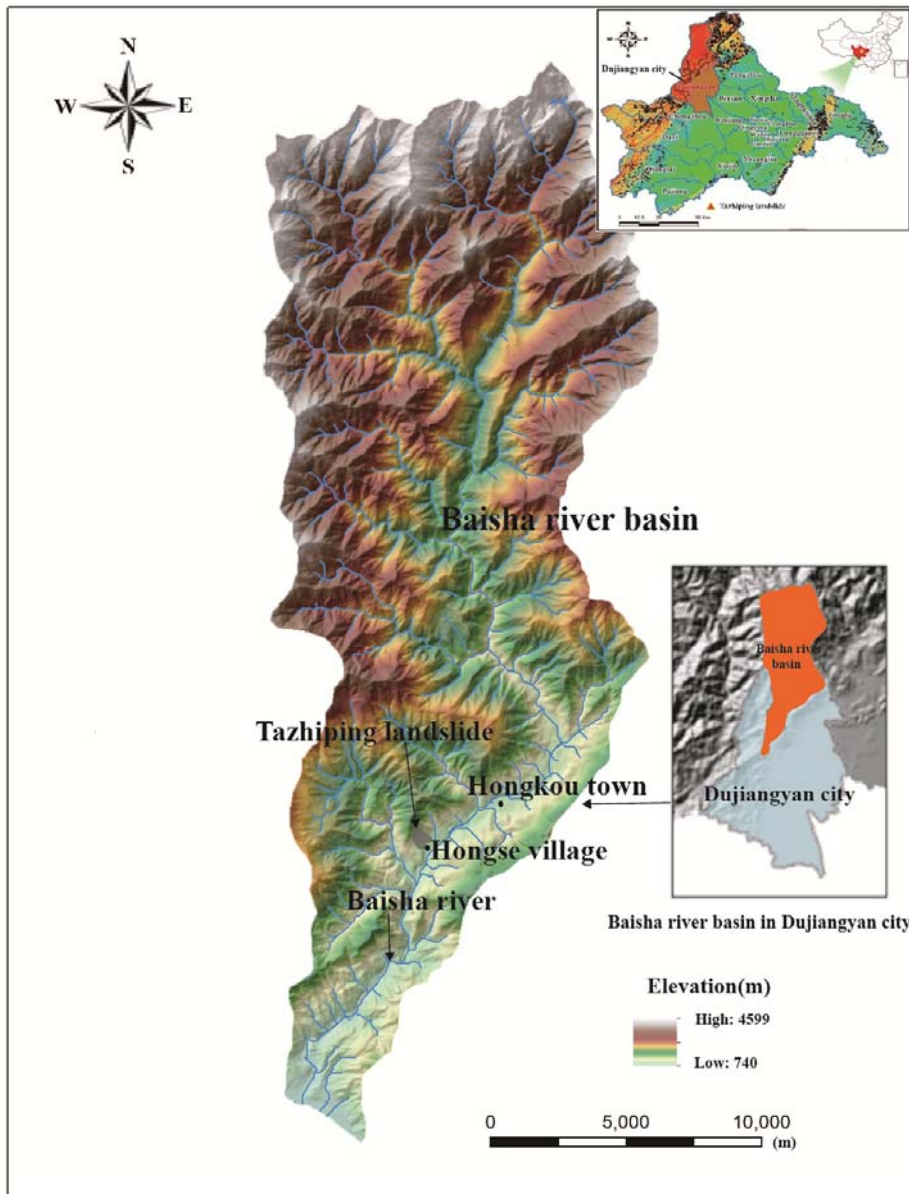
206 3. Study area and data

207 3.1 Taziping landslide

208 The Taziping landslide is located southeast of the Hongse Village, Hongkou
 209 Town, Dujiangyan City of Sichuan Province. The site is located at (E103°37'46",
 210 N31°6'29"), 68 km west Chengdu City and 20 km from the Dujiangyan Urban
 211 District (Fig. 2). Its geomorphic unit is a middle-mountain tectonic erosional area on
 212 the north bank of the Baisha River Valley. The Taziping Landslide is a large-scale
 213 colluvial layer landslide triggered by the Wenchuan Earthquake (Fig. 3). It has a
 214 gradient of 25°-40° with an average gradient of 32°. The landslide has an apparent
 215 round-backed armchair contour with a steep rear edge, which has a gradient of
 216 35°-50° and an elevation of about 1,370 m. The front edge is located on the south side
 217 of the mountain road, and has an elevation of about 1,007 m. The landslide has an

[a4]: Answer to the comment Q5: We have introduced the method used to do the hazard prediction and the evaluation of the dynamic interaction with buildings.

218 elevation difference of about 363 m, and a main sliding direction of 124°NE. The
219 landslide mass forms an irregular semi-elliptical shape, and has a length of about 530
220 m, an average width of 145 m and an area of approximately $7.68 \times 10^4 \text{ m}^2$. The
221 landslide mass is composed of gravelly soil and is covered on by silty clay mingled
222 with gravel. In terms of spatial distribution, the landslide is thick in the middle and
223 thin on the lateral edges, has a thickness of 20-25 m and a volume of approximately
224 $1.16 \times 10^6 \text{ m}^3$. During the earthquake, the landslide mass slid to cover the northern
225 mountain slope of the Hongse Village Miaoba settlement. The landslide has an
226 apparent front edge boundary, and there is also a swelling deformation (Fig. 4).

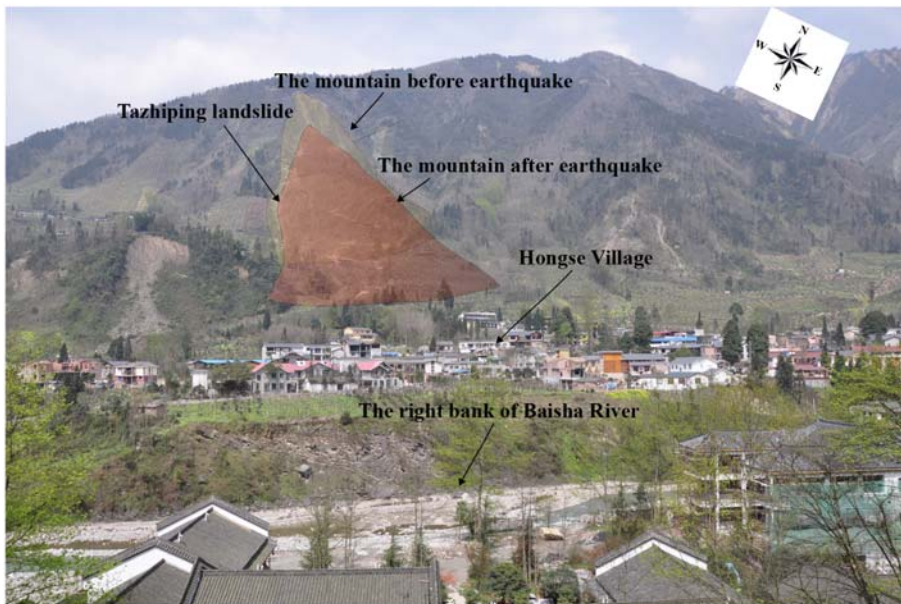


227

228

229

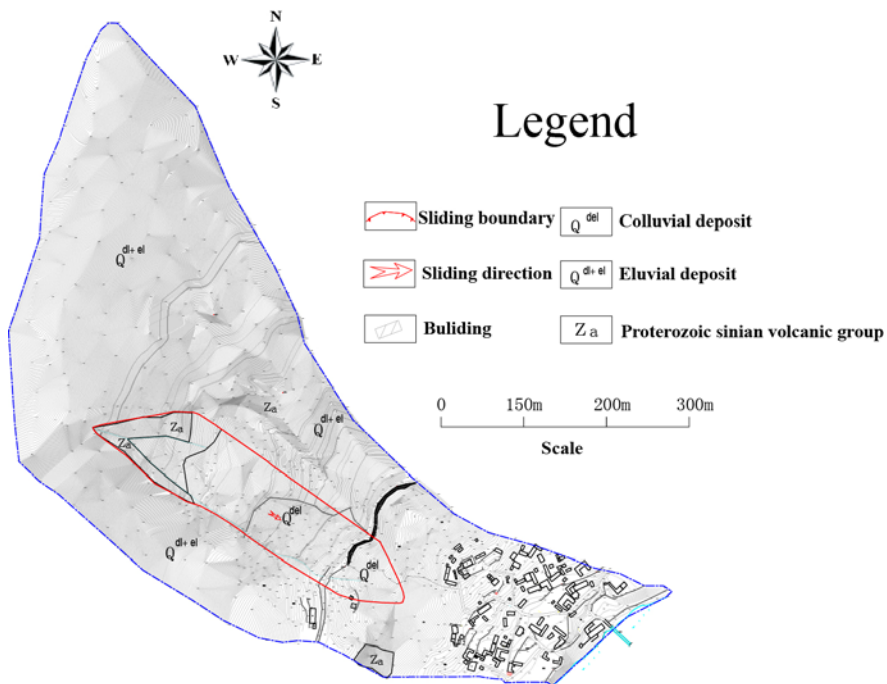
Fig.2 Location of Tazhiping landslide, Baisha river basin, Dujiangyan city (the landslide was triggered by Wenchuan Ms 8.0 earthquake on May 12, 2008)



230

231

Fig.3 Tazhiping Landslide



232

233

234

235

236

Fig.4 Plane sketch of the Tazhiping landslide

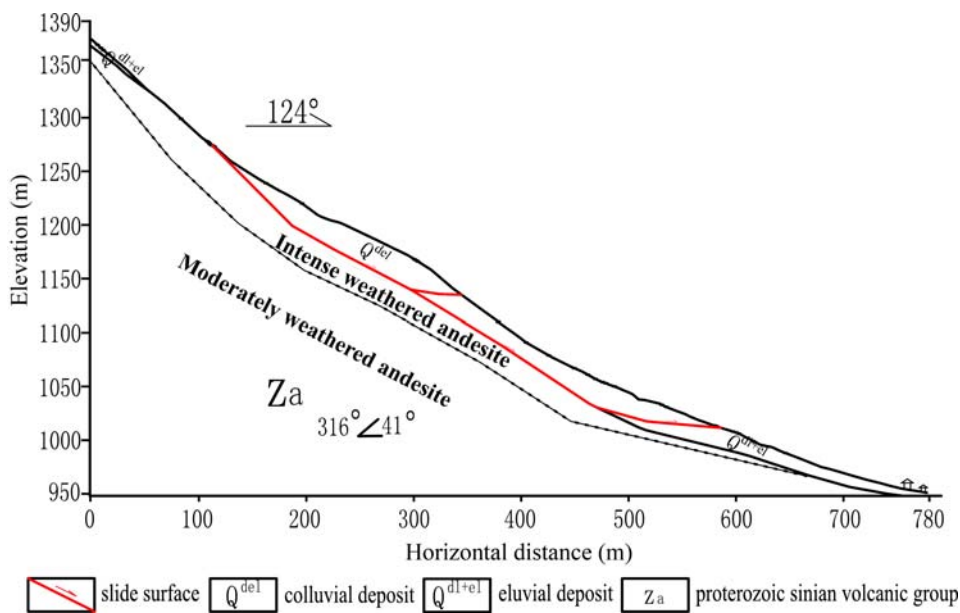
After the Wenchuan Earthquake, the massive colluvial deposits covered the mountain slope. The colluvium is 0.5-5.0 m thick at the top of the slide and is composed of rubble and gravel. The mass consists of a small amount of fine gravel,

[a5]: Answer to the comment Q6: It is based on the survey report and field investigation.

237 which is composed of gray or grayish-green andesite with a clast of 20-150 cm. Field
 238 surveys indicate that the rubble in the surface layer has a maximum diameter
 239 exceeding 2 m, and that fine gravel is loosely intercalated with the rubble. A small
 240 amount of yellowish-brown and gray-brown silty clay mixed with 5-40% of
 241 non-uniformly distributed rubble composed the first 5-10 m of the slide. From 10-25
 242 m deep, there is a wide distribution of gravelly soil. The soil is grayish-green or
 243 variegated in color, is slightly compact and non-uniform, and has a rock fragment
 244 content of about 50%. The parent rock of the rock fragments is andesite, filled with
 245 silty clay or silt (Fig.5). Table 1 shows the parameters of the surface gravelly soil of
 246 the landslide mass based on the field sampling.

247 Tab.1 Parameters of surface soil of Taziping Landslide

Internal friction angle (°)		Cohesion (kPa)	Relative compactness	Natural void ratio	Dry density (kN·m ⁻³)	Specific gravity (g·cm ⁻³)
Peak	Residual					
27.5	23	20.5	53%	0.789	15.357	2.492



248

249 Fig.5 Geological profile of the Taziping Landslide

250 The landslide is an unconsolidated mass containing relatively large amounts of
 251 crushed stones and silty clay (Fig.6). Its loose structure and strong permeability
 252 facilitate infiltration of surface water. The Wenchuan earthquake aggravated the
 253 deformation of the landslide making deposits more unconsolidated, further reducing
 254 the stability of the landslide mass. During persistent rainfall, surface water infiltrates
 255 the landslide slope resulting in increased water pressure within the landslide mass and

256 reduced shear strength on the sliding surface. Thus, rainfall constitutes the primary
257 inducing factor of the upper Taziping landslide. After infiltrating the loose layer, water
258 saturates the slope increasing the dead weight of the sliding mass and reducing the
259 shear strength of soil in the sliding zone. Infiltration into the landslide mass also
260 increases the infiltration pressure of perched water, drives deformation, and poses a
261 great threat to villages located at the front of the landslide. Slide-resistant piles and
262 backfill were placed at the toe of the slope in order to reduce the hazards of future
263 slides. The slide-resistant piles have enhanced the overall stability of the slope,
264 however, under heavy rainfall the upper unconsolidated landslide deposits may cut
265 out from the top of the slide-resistant piles.



266

267 (a) Material on the landslide surface (b) Material in the shear zone

268 Fig.6 Photographs showing colluvial deposit cover on the mountain slope

269 Therefore we simulate possible movement states of the Taziping landslide before
270 and after treatment with slide-resistant piles, comparatively analyzed the kinetic
271 parameters in the movement process, and mapped the 2D division of hazard zones.

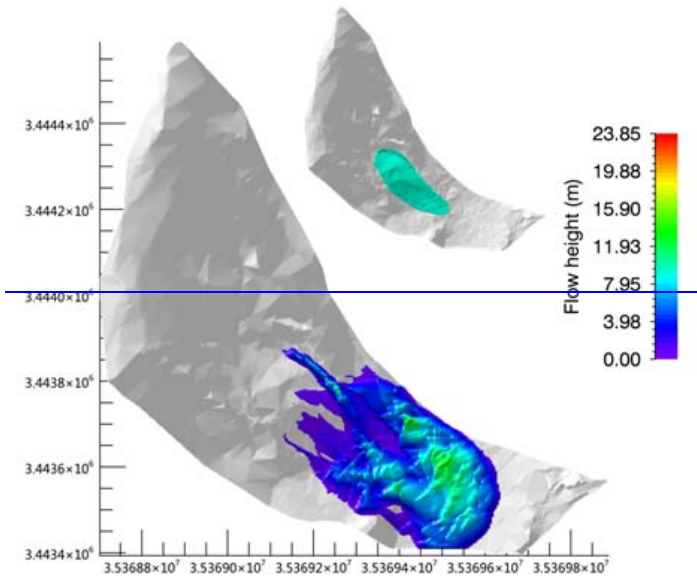
272

273 3.2 Hazard prediction before treatment

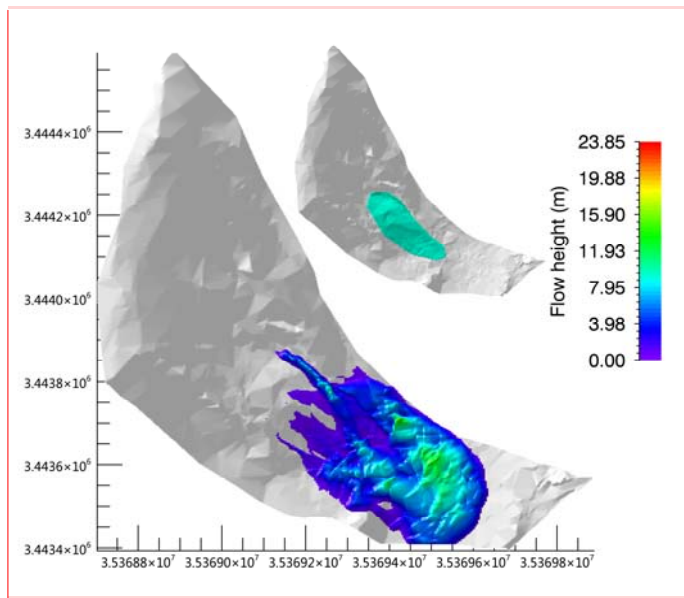
274 It was assumed that the landslide was damaged before engineering treatment.
275 According to field investigation, the sliding mass had an estimated starting volume of
276 about $600,000\text{m}^3$ and a mean thickness of 8m. Based on the survey report and field
277 investigation (Hydrologic Engineering and Geological Survey Institute of Hebei
278 Province, 2010), we adopted the survey parameters of Tab.2 for the simulated
279 calculation. These parameters were obtained from laboratory or small-scale
280 experiments and back-analyses of relatively well-documented landslide cases. The
281 unit weigh $\gamma = 20.8\text{kN} \cdot \text{m}^{-3}$ is from small-scale conventional
282 triaxial test experiments in laboratory. In addition, we selected the coulomb friction
283 coefficient $\mu = 0.45$ and viscous friction coefficient $\zeta = 500\text{m} \cdot \text{s}^{-2}$ in accordance
284 with back-analyses of well-documented landslide cases (Cepeda et al., 2010; Du et al.,
285 2015). The erosional entrainment rate selected was the minimum value $k_i = 0.0001$
286 in the RAMMS program.

Tab.2 Model calculation parameters

Unit weight $\gamma(kN \cdot m^{-3})$	Coulomb friction coefficient μ	Viscous friction coefficient $\zeta(m \cdot s^{-2})$	Erosional entrainment rate k_i
20.8	0.45	500	0.0001



288

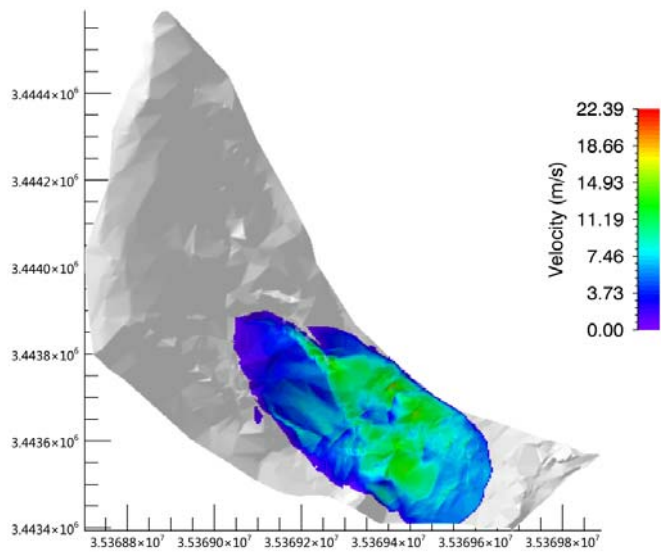


289

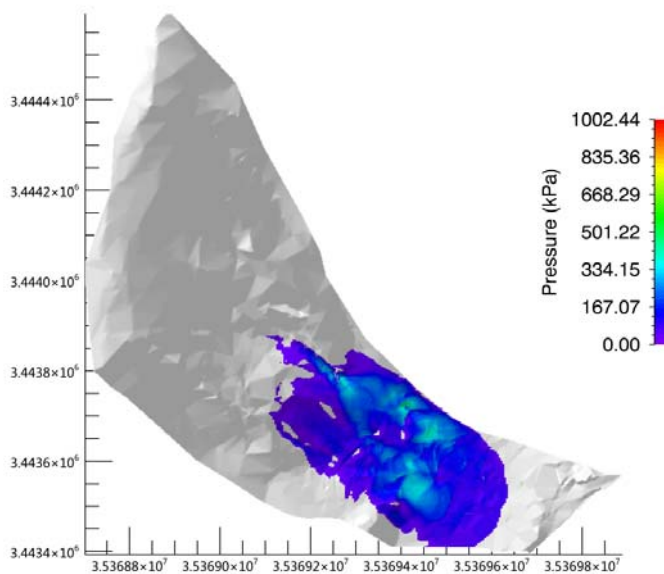
290

(a) Flow height

[a6]: Answer to the comment Q2: This figure has been improved.



(b) Velocity



(c) Pressure

Fig. 7 Movement characteristic parameters of the Taziping landslide (before treatment)

See the kinematic characteristic parameters of the landslide deposits in Fig.7. The colored bar shows the maximum values of the kinematic process for a given time step. As shown by the calculation results, deposits accumulated during the landslide movement process had a maximum flow height of 23.85m, located around the surface

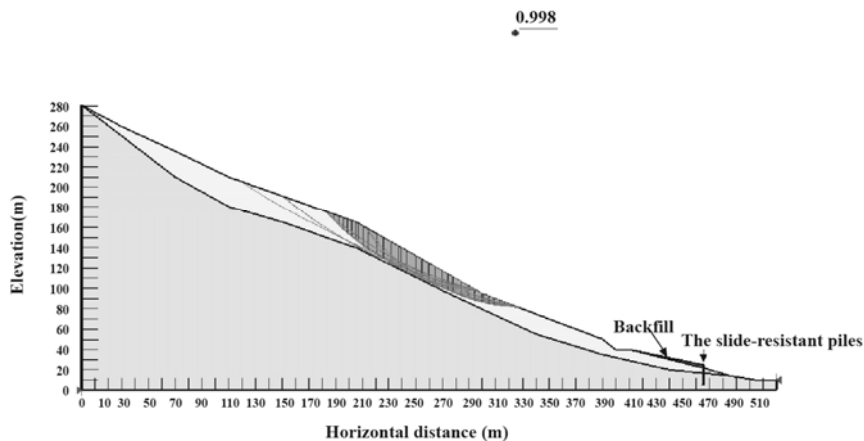
301 gully of the middle and upper slope. The middle and lower section— of the landslide
302 deposit had a flow height of about 5-10m; the middle and lower movement speed
303 velocity of the landslide ranged from 3m/s and 7m/s; the landslide had a mean
304 pressure of about 500kPa, and the pressure of the middle and lower deposits was
305 about 200kPa. Thus, three-story and lower houses within the deposition range might
306 be buried (The building is 3m high on each floor), and it was further suggested that
307 the design strength of the gable walls of houses on the middle and upper parts of the
308 deposit be increased above 300kPa.

309

310 3.3 Hazard prediction after treatment

311 After fully accounting for the slide-resistant piles and mounds, we introduced the
312 Morgenstern-Price method (Morgenstern et al., 1965) to calculate the stability
313 coefficient of Taziping landslide after treatment. The method was determined with an
314 iterative approach by changing the position of the sliding surface until failure of the
315 dumpsite (Fig.8). The physico-mechanical parameters under a saturated state
316 (Hydrologic Engineering and Geological Survey Institute of Hebei Province, 2010)
317 were adopted to search for the sliding plane of the landslide.

318

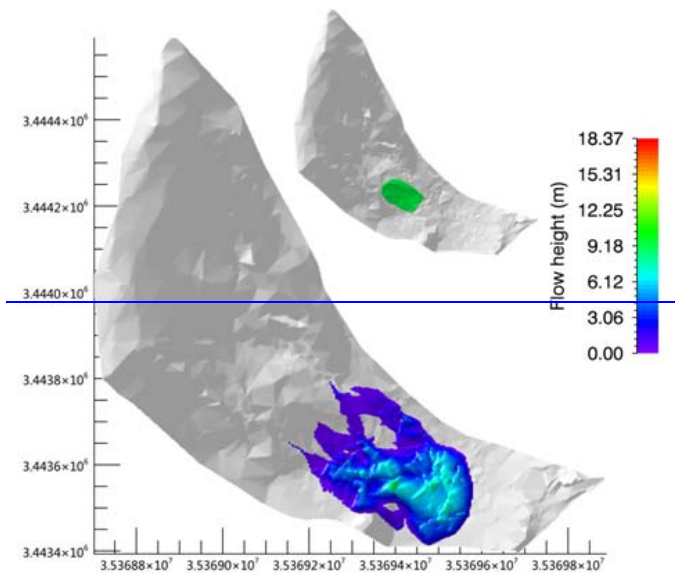


319 Fig.8 Search for the sliding plane of the Taziping landslide (before treatment)

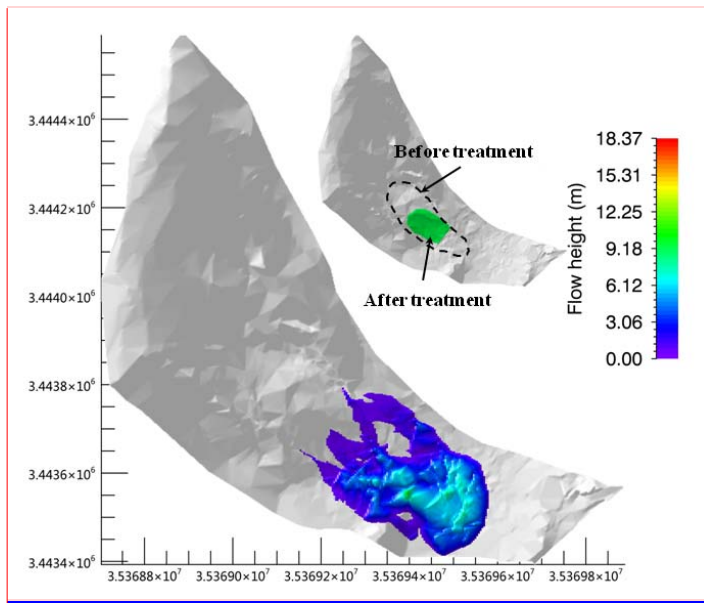
320 Based on numerical analysis, the Taziping landslide stability coefficient is 0.998.
321 Under rainfall conditions, the middle area of the Taziping landslide was unstable.
322 Loose deposits in the middle part of the landslide might convert into a high-water
323 landslide and cut out from the top of the slide-resistant piles. In the damaged area, the
324 slope had a rear edge wall elevation of about 1,170m. Its front edge was located on
325 the south side of the mountain road, with an elevation of 1,070-1,072m and a length
326 of 182m. Thus, the scale of the rainfall-damaged is estimated to be about 250,000m³,
327 with a mean thickness of about 6m. The parameters in Tab.2 were again adopted for
328 the simulated calculation.

[a7]: Answer to the comment Q7: It has been deleted and deleted the blanks between words in the line above.

329



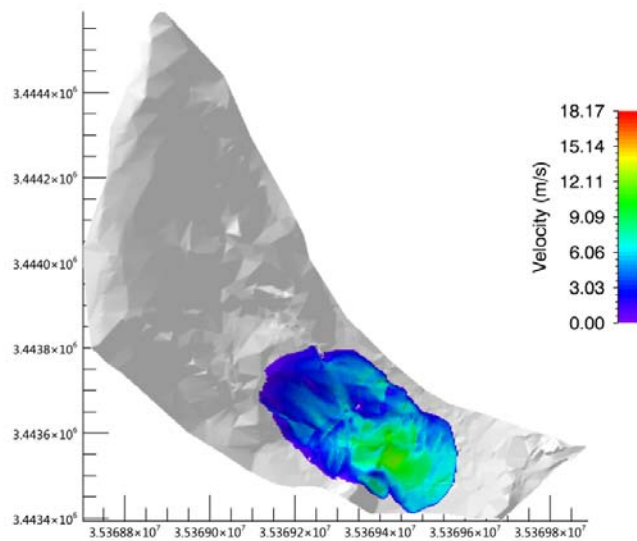
330



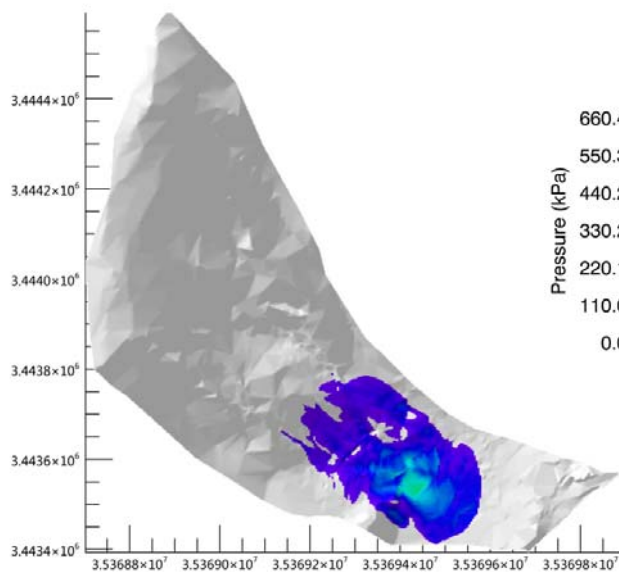
331

(a) Flow height

[a8]: Answer to the comment Q2 and Q7: This figure has been improved and added more information about the comparison between model result and reality.



(b) Velocity



(c) Pressure

Fig. 9 Movement characteristic parameters of the Taziping landslide (after treatment)

Provided in Fig.9 are the kinematic characteristics of the landslide deposit. The colored bar shows the maximum values of the kinematic process for a given time step. Deposits accumulated during the landslide movement process had a maximum flow height of 18.37m, located around the surface gully of the middle and upper slope. The middle and lower portions of the landslide deposit had a flow height of approximately 3-5m. The middle and lower movement velocity of the landslide deposits ranged

343 between 3m/s and 5m/s. The landslide had a mean pressure of about 330kPa, and the
 344 pressure of the middle and lower deposits was about 100kPa. Thus, it could be held
 345 that two-story and lower houses within the deposition range might be buried. It was
 346 further suggested that the design strength of the gable walls of houses on the middle
 347 and upper parts of the deposits be increased above 150kPa.

348 After treatment, the accumulation flow height and pressure of the deposits were
 349 reduced by about 1/2, and the kinematic speed is reduced by about 1/3. However, the
 350 Miaoba residential area of Red Village was still partially at hazard.

351

352 4 Results

353 Landslides reflect landscape instability that evolves over meteorological and
 354 geological timescales, and they also pose threats to people, property, and the
 355 environment. The severity of these threats depends largely on landslide speed and
 356 travel distance. There may be examples where entire houses on a landslide mass are
 357 moved but not destroyed because of stable base plates. In any case, velocity plays a
 358 more important role regarding kinetic energy acting on an obstacle. However, the
 359 Miaoba residential area of Red Village is located at the frontal part of Tazhiping
 360 landslide. During landslide movement, the spatial scale indexes of a landslide mass
 361 include area, volume, and thickness. The maximum thickness of the landslide is one
 362 of the direct factors influencing the building's deformation failure status. A large
 363 landslide displacement may lead to burial, collapse, or deformation failure of the
 364 building, and thus influence its safety and stability. Thus, landslide thickness
 365 constitutes an important index for assessing the hazards of a landslide disaster, and for
 366 influencing the consequences faced by disaster-affected bodies (Fell et al., 2008;
 367 DZ/T, 0286-2015). Provided in Tab.3 is a landslide thickness-based division of the
 368 predicted hazard zones of Tazhiping landslide, in which the thickness of the landslide
 369 mass correlates with the ability of a building to withstand a landslide disaster (Hung
 370 et al., 1984; Petrazzuoli et al., 2004; Glade 2006; GB, 50010-2010; Hu et al., 2012;
 371 Zeng et al., 2015). After treatment with slide-resistant piles, the hazard of a future
 372 slide was reduced by about 1/3 overall and by 2/3 in high-hazard zones.

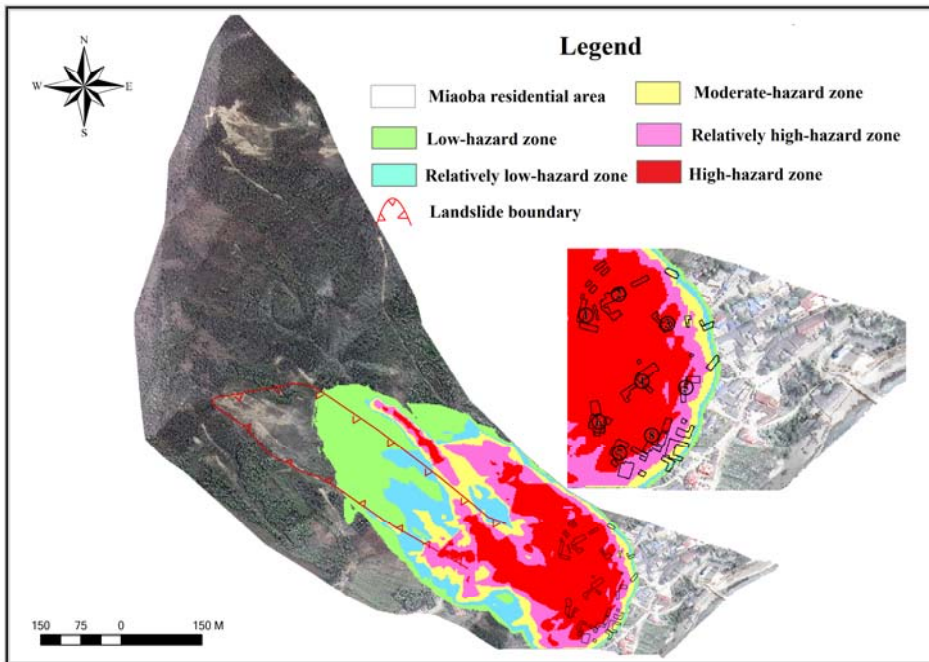
373 **Tab.3 Division table of the predicted hazards of Tazhiping landslide (unit: m²)**

Hazard zone level	Assessment index	Building damage probability	Area before treatment	Area after treatment	Increased/decreased area	Building damage characteristics
Low-hazard zone (I)	$h \leq 0.5m$	20%	44 , 600	38 , 748	-5,852	One-story houses may be damaged; houses on the

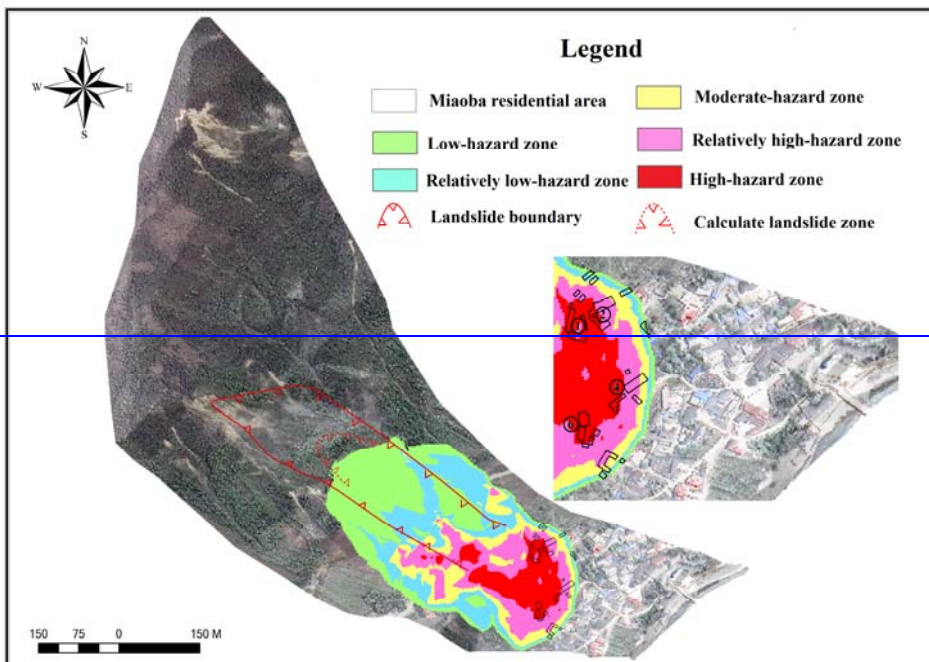
						landslide mass are partially damaged.
						One-story houses have a very high probability of being damaged; one-story houses on the landslide mass are completely damaged.
Relatively low-hazard zone (II)	$0.5\text{ m} < h \leq 1\text{ m}$	50~20%	24 , 900	26 , 400	+1,500	One-story to three-story houses have a very high probability of being damaged; houses less than three stories on the landslide mass are completely damaged.
Moderate-hazard zone (III)	$1\text{ m} < h \leq 3\text{ m}$	80~50%	21 , 980	15 , 856	-6,124	One-story houses may be buried, and two-story to six-story houses have a very high probability of being damaged; houses on the landslide mass are completely
Relatively high-hazard zone (IV)	$3\text{ m} < h \leq 5\text{ m}$	100~80%	30 , 820	19 , 636	-11,184	are completely

						damaged.
						Two-story and
						lower houses may
						be buried, and
						three-story and
						higher houses have
High-hazard						a very high
zone	$h \geq 5m$	100%	47 , 240	13 , 052	-34,188	probability of being
(V)						damaged; houses on
						the landslide mass
						are completely
						damaged.
Total area:	—	—	169 , 540	113 , 700	-54,340	—

374 The hazard zones of Taziping landslide was given by 2D divisions before and
375 after engineering treatment (Fig. 10). The size of the hazard zones changed after
376 engineering treatment, particularly in the high-hazard zones. Before treatment with
377 slide-resistant piles, the landslide posed a great hazard to eight houses on the left side
378 of the upper Miaoba residential area, with a high-hazard zone associated with
379 landslide mass height over 5m and a red zone. After treatment, the number of effected
380 houses was reduced to four. We defined outside the colored area as no-hazard.



(a) Before treatment



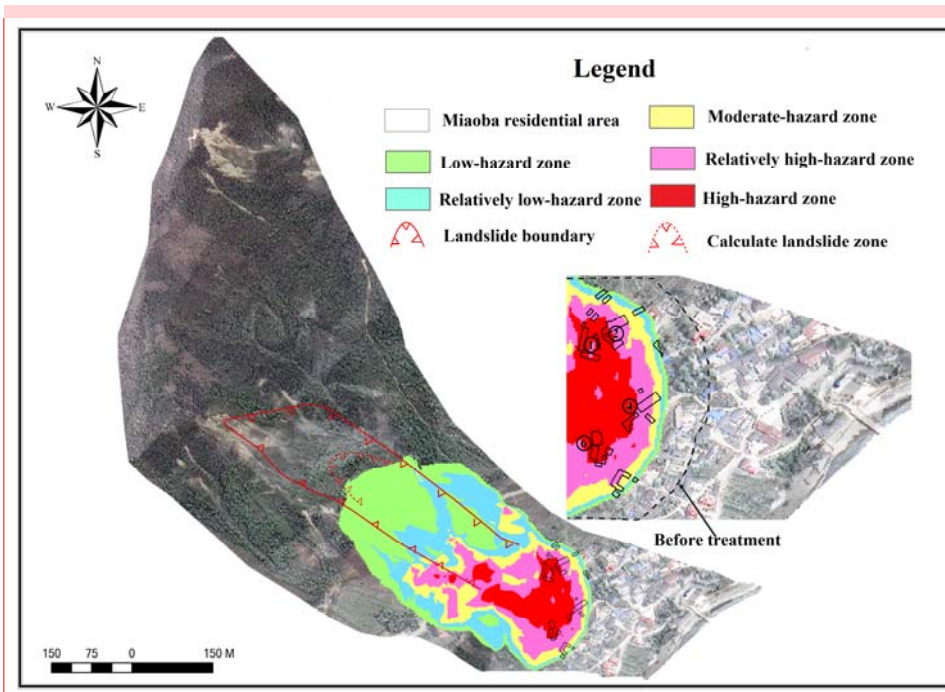
381

382

383

384

385



(b) After treatment

Fig. 10 2D division comparison of the hazards of the Taziping landslide

5 Conclusions and Discussion

The hazard assessment of landslides using numerical models is becoming more and more popular as new models are developed and become available for both scientific research and practical applications. There is some confusion about the mass movement process that is discussed by the rheological model presented in this contribution.

Landslides move downslope in many different ways (Varnes, 1978). In addition, landslides can evolve into rapidly travelling flows, which exhibit characteristics of debris flows on unchannelized or only weakly channelized hillslopes. The geomorphic heterogeneity of rapid shallow landslides, such as hillslope debris flows, is larger than observed in channelized debris flows; however many of these flows can be successfully modelled using the Voellmy-fluid friction (Christen et al., 2012). Results presented in this paper support the conclusion that Voellmy-fluid rheological model can be used to simulate flow-type landslides.

The selection of model parameters remains one of the fundamental challenges for numerical calculations of natural hazards. At present, there are numerous empirical parameters obtained from 30-years of monitoring data. Such as in RAMMS, we can automatically generate the friction coefficient of an avalanche for our calculation domain based on topographic data analysis, forest information and global parameters (WSL, 2013). The friction parameters for debris flows can found in some literature (Fannin et al., 2001; Iovine et al., 2003; Hürlimann et al., 2008; Scheidl et

[a9]: Answer to the comment Q2 and Q7: We have re-organized and added more information about the comparison between pre and post treatment results could be solved easily introducing some additional lines of main results from the pre simulations in the figures of the post simulations.

[a10]: Answer to the comment Q8: We have move p. 20 lines 373 - 380 to the section "Empirical prediction method" and repeat it partially in the conclusions.

411 al., 2010; Huang et al., 2015). However, there is little research regarding friction
412 parameters of flow-type landslide. Therefore, we tested different coulomb friction
413 coefficient μ values ranging between $0.1 \leq \mu \leq 0.6$ and viscous friction coefficient ζ
414 values ranging between $100 \leq \mu \leq 1000 m \cdot s^{-2}$. Finally, we selected the coulomb
415 friction coefficient $\mu = 0.45$ and viscous friction coefficient $\zeta = 500 m \cdot s^{-2}$ in
416 accordance with back-analyses of well-documented landslides (Cepeda et al., 2010;
417 Du et al., 2015). Simulation results are consistent with field observations of
418 topography and sliding path.

419 Based on the finite volume method and the RAMMS program, simulation results
420 of Taziping landslide were consistent with the sliding path predicted by the field
421 investigation. This correlation indicates that numerical simulation is an effective
422 method for studying the movement processes of flow-type landslides. The
423 accumulation flow height and pressure of landslide deposits were reduced by about
424 1/2, and the kinematic speed was reduced by about 1/3 after treatment. However, the
425 Miaoba residential area of Red Village is still partially at hazard. Considering that
426 two-story and lower houses within the deposition range might be buried, it was further
427 suggested that the design strength of the gable walls of houses on the middle and
428 upper parts of the deposit be increased above 150kPa.

429 By utilizing a GIS platform in combination with landslide hazard assessment
430 indexes, we mapped the 2D division of the Taziping landslide hazard zones before
431 and after engineering treatment. The results indicated that overall hazard zones
432 contracted after engineering treatment and, the area of high-hazard zones was reduced
433 by about 2/3. After engineering treatment, the number of at hazard houses on the left
434 side of the upper Miaoba residential area, was reduced from eight to four. It was thus
435 clear that some zones are still at high hazard despite engineering treatment. Therefore,
436 it was proposed that houses located in high-hazard zones be relocated or reinforced
437 for protection.

438
439
440

441 **Acknowledgments**

442 The authors sincerely acknowledge the CAS Pioneer Hundred 432 Talents
443 Program for the completion of this research. This work was supported by National
444 Natural Science Foundation of China (Grant No. 41301009 41301592) and the
445 Hundred Young Talents Program of IMHE (SDSQB-2016-01), the International
446 Cooperation Program of the Ministry of Science and Technology of China (Grant
447 No.2013DFA21720). The authors express their deepest gratitude to those aids and
448 assistances. The authors also extend their gratitude to editor and two anonymous
449 reviewers for their helpful suggestions and insightful comments, which have
450 contributed greatly in improving the quality of the manuscript.

451

452

453

454 **Reference**

- 455 Bartelt, P., Bühler, Y., Buser, O., Christen, M., and Meier, L.: Modeling mass-dependent flow
456 regime transitions to predict the stopping and depositional behavior of snow avalanches, *J.*
457 *Geophys. Res.*, 117, F01015, doi:10.1029/2010JF001957, 2012 .
- 458 Costa, J.E.: Physical geomorphology of debris flows. *Developments and Applications of*
459 *Geomorphology*, Springer Press., 268-317, 1984.
- 460 Christen, M., Kowalski, J., and Bartelt, P.: RAMMS: Numerical simulation of dense snow
461 avalanches in three-dimensional terrain, *Cold Regions Science and Technology.*, 63, 1–14,
462 2010.
- 463 Christen, M., Bartelt, P., and Kowalski, J.: Back calculation of the In den Arelen avalanche with
464 RAMMS: interpretation of model results, *Annals of Glaciology.*, 51, 161–168, 2010.
- 465 Christen, M., Bühler, Y., Bartelt, P., Leine, R., Glover, J., Schweizer, A., Graf, C., McArdeell, B.,
466 Gerber, W., Deubelbeiss, Y., Feistl, T., and Volkwein, A.: Integral hazard management using a
467 unified software environment: numerical simulation tool “RAMMS” for gravitational natural
468 hazards, In: Koboltschnig, G., Hübl, J., Braun, J. (eds.) *Proceedings of 12th Congress*
469 *INTERPRAE.*, 1, 77–86, 2012.
- 470 Chen, J.C., and Chuang, M.R.: Discharge of landslide-induced debris flows: case studies of
471 Typhoon Morakot in southern Taiwan, *Nat. Hazards Earth Syst. Sci.*, 14, 1719-1730, 2014.
- 472 Cepeda, J., Chávez, J.A., and Martínez, C.C.: Procedure for the selection of runout model
473 parameters from landslide back-analyses: application to the Metropolitan Area of San
474 Salvador, El Salvador, *Landslides.*, 7, 105–116, 2010.
- 475 Du, J., Yin, K.L., and Wang, J.J.: Simulation of three-dimensional movement of landslide-debris
476 flow based on finite volume method, *Chinese Journal of Rock Mechanics and Engineering.*,
477 34: 480–488, 2015 (in Chinese).
- 478 Evans, S.G., Tutubalina, O.V., Drobyshev, V.N., Chernomorets, S.S., McDougall, S., Petrakov,
479 D.A., and Hungr, O.: Catastrophic detachment and high-velocity long-runout flow of Kolka
480 Glacier, Caucasus Mountains, Russia in 2002, *Geomorphology.*, 105, 314–321, 2009.
- 481 Fannin, R.J., and Wise, M.P.: An empirical-statistical model for debris flow travel distance,
482 *Canadian Geotechnical Journal.*, 38, 982–994, 2001.
- 483 Finlay, P.J., Mostyn, G.R., and Fell, R.: Landslide risk assessment: prediction of travel distance,
484 *Canadian Geotechnical Journal.*, 36, 556–562, 1999.
- 485 Fell, R., Corominas, J., Bonnard, C., Cascini, L., Leroi, E., and Savage, W. Z.: Guidelines for
486 landslide susceptibility, hazard and risk zoning for land use planning, *Engineering Geology.*,
487 102, 85–98, 2008.
- 488 Fannin, R., and Wise, M.: An empirical-statistical model for debris flow travel distance, *Can*
489 *Geotech J.*, 38, 982–994, 2001.
- 490 Glade, T.: Linking debris-flow hazard assessments with geomorphology. *Geomorphology.*, 66(1):
491 189-213, 2005.
- 492 Glade, T., Anderson, M. G., Crozier, M.J.: *Landslide hazard and risk.* Wiley., 75-138, 2006.
- 493 GB 50010–2010.: *Code for design concrete structures*, Beijing: Chinese Architectural Industry.,
494 34–80, 2010 (in Chinese).
- 495 Hebei Province Institute of Hydrogeological and Engineering.: *Geological investigation*

496 engineering supplemental survey report of Hongse Village Taziping landslide in Hongkou
497 Town of Dujiangyan City, Sichuan Province., 2010 (in Chinese).

498 Hungr, O.: A Model for the runout analysis of rapid flow slides, debris flows and avalanches, *Can*
499 *Geotech J.*, 32, 610–623, 1995.

500 Hungr, O., Evans, S.G., Bovis, M.J., and Hutchinson, J.N.: A review of the classification of
501 landslides of the flow type, *Environ Eng Geosci.*, 7, 221–238, 2001.

502 Hungr, O., Morgan G.C., and Kellerhals, R.: Quantitative analysis of debris torrent hazards for
503 design of remedial measures, *Can Geotech J.*, 21, 663–677, 1984.

504 Hu, K.H., Cui, P., and Zhang, J.Q., Characteristics of damage to buildings by debris flows on 7
505 August 2010 in Zhouqu, Western China, *Nat Hazards Earth Syst Sci.*, 12, 2209–2217, 2012.

506 Hürlimann, M., Rickenmann, D., Medina, V., and Bateman, A.: Evaluation of approaches to
507 calculate debris-flow parameters for hazard assessment, *Eng Geol.*, 102, 152–163, 2008.

508 Huang, Y., Cheng, H., Dai, Z., Xu, Q., Liu, F., Sawada, K., Moriguchi, S., and Yashima, A.:
509 SPH-based numerical simulation of catastrophic debris flows after the 2008 Wenchuan
510 earthquake, *Bull Eng Geol Environ.*, 74, 1137–1151, 2015.

511 Iverson, R. M., Reid, M. E., and LaHusen, R. G.: Debris-flow mobilization from landslides, *Annu.*
512 *Rev. Earth Planet Sc.*, 25, 85– 138, 1997.

513 Iverson, R.M., and Vallance, J.W.: New views of granular mass flows, *Geology.*, 29, 1115–1118,
514 2001.

515 Iovine, G., Gregorio, S.D., and Lupiano, V.: Debris-flow susceptibility assessment through cellular
516 automata modeling: an example from 15–16 December 1999 disaster at Cervinara and San
517 Martino Valle Caudina (Campania, southern Italy), *Nat Hazards Earth Syst Sci.*, 3, 457–468,
518 2003.

519 Jackson, L.E., Kostashuk, R.A., and MacDonald, G.M.: Identification of debris flow hazard on
520 alluvial fans in the Canadian Rocky mountains, *Geological Society of America.*, 7, 155–124,
521 1987.

522 LeVeque, R.: *Finite Volume Methods for Hyperbolic Problems*, Cambridge Texts in Applied
523 *Mathematics* Cambridge University Press., 2002.

524 Michael-Leiba, M., Baynes, F., Scott, G., and Granger, K.: Regional landslide risk to the Cairns
525 community, *NatHazards.*, 30, 233–249, 2003.

526 Morgenstern, N.R., and Price, V.E.: The analysis of the stability of general slip surfaces,
527 *Geotechnique.*, 15, 79–93, 1965.

528 Portilla, M., Chevalier, G., and Hürlimann, M.: Description and analysis of the debris flows
529 occurred during 2008 in the Eastern Pyrenees, *Nat. Hazards Earth Syst. Sci.*, 10, 1635–1645,
530 2010.

531 Petrazzuoli, S.M., and Zuccaro, G.: Structural resistance of reinforced concrete buildings under
532 pyroclastic flows: a study of the Vesuvian area, *J Volcanol Geoth Res.*, 133, 353–367, 2004.

533 Sassa, K., Nagai, S., Solidum, R., Yamazaki, Y., and Ohta, H.: An integrated model simulating the
534 initiation and motion of earthquake and rain induced rapid landslides and its application to
535 the 2006 Leyte landslide, *Landslides.*, 7, 219–236, 2010.

536 Scott, K.M., and Vallance, J.W.: *History of Landslides and Debris Flows at Mount Rainier: Water*
537 *Fact Sheet*, USGS Open-File Report., 93–111, 1993.

538 Shi, G.H.: *Discontinuous deformation analysis - a new numerical model for the statics and*
539 *dynamics of block system*, Berkeley: University of California., 1988.

540 DZ/T 0286-2015.: Specification of risk assessment for geological hazard, Ministry of Land and
541 Resources of the People's Republic of China., 2015 (in Chinese).

542 Scheidl, C., and Rickenmann, D.: Empirical prediction of debris-flow mobility and deposition on
543 fans, *Earth Surf Proc Land.*, 35, 157–173, 2010.

544 Toro, E.F.: Riemann problems and the waf method for solving the two dimensional shallow water
545 equations. *Philos. Trans. R. Soc. London., Ser. A* 338, 43–68, 1992.

546 Varnes, D.J., : Slope movement types and processes. In: Schuster RL, Krizek RJ (eds) *Landslides:
547 analysis and control*. Transportation Research Board, National Research Council, Washington,
548 DC, USA., 11–33 , 1978.

549 Wang, L., Li, B., Gao, Y., and Zhu, S.: Run-out prediction of large thick-bedded unstable rock: A
550 case study of Daxiang unstable rock in Yangjiao town, Wulong county, Chongqing, *Earth
551 Science Frontiers.*, 23, 251–259, 2016 (in Chinese).

552 WSL.: *RAMMS: A numerical model for snow avalanches in research and practice*, User manual
553 v1.5 avalanche, WSL Institute for snow and avalanche research SLF, Swiss., 2013.

554 Zeng, C., Cui, P., Su, Z.M., Lei, Y., Chen, R.: Failure modes of reinforced concrete columns of
555 buildings under debris flow impact, *Landslides.*, 12, 561-571, 2015.